CCFE
CULHAM CENTRE FOR FUSION ENERGY

UK Atomic Energy Authority

UKAEA-CCFE-PR(25)332

M. Yu. Lavrentiev, N. L. Allan, O. Hawkins

Disorder and damage recovery in irradiated lithium oxide

Disorder and damage recovery in irradiated lithium oxide

M. Yu. Lavrentiev, N. L. Allan, O. Hawkins

This is a preprint of a paper submitted for publication in
Physics Chemistry Chemical Physics

Disorder and damage recovery in irradiated lithium oxide

M. Yu. Lavrentiev[1], N. L. Allan[2], and O. Hawkins[2]

[1]United Kingdom Atomic Energy Authority, Culham Campus, Abingdon, Oxon, OX14 3DB, UK

[2]School of Chemistry, University of Bristol, Bristol BS8 1TS, UK

Abstract

We assess the disorder created in lithium oxide, an important candidate material for tritium breeding in fusion nuclear reactors, by high-energy neutron bombardment. Steinhardt order parameters distinguish the different local environments of Li ions in the damaged structure, differentiating between interstitial and lattice sites. The order parameters are also used to determine the evolution of the damage with time. We estimate the time needed for healing to return to the pre-damaged structure over a range of temperatures and show that this is at a minimum at temperatures close to the working conditions of a breeding blanket.

I. Introduction

Commercial fusion power plants will only be viable if tritium spent in a fusion reaction can be replaced by tritium bred in the breeder section of the power plant. Breeding can be achieved by the reactions of the isotopes ^{6}Li and ^{7}Li with neutrons. Thus, lithium compounds and, in particular, lithium oxide, Li_2O, are the most promising materials for obtaining uninterrupted tritium fuel cycle [1-4]. During the life of the power plant, breeder material will be subject to high neutron fluxes that will create damage cascades and ultimately introduce large number of defects into the crystal structure. Hence there is a vital need to be able to understand damage in Li_2O quantitatively and to predict the level of damage under typical working conditions.

Li_2O has the antifluorite structure (space group $Fm\bar{3}m$). The Li atoms by themselves form a simple cubic lattice and the O atoms a face-centred cubic lattice; the cubic unit cell contains four O and eight Li atoms (see Figure 1). The lattice parameter a_0 varies between 4.6 and 4.8 Å over the temperature range 0 – 1500 K [5-8]; the shortest Li-Li distance, d, increases from 2.3 to 2.35 Å over this range.

In this paper, we use molecular dynamics simulations and Steinhardt order parameters [9] to investigate how the lithium and oxygen sublattices change on irradiation. Simulations are performed at several temperatures, including a low temperature (500 K), a temperature (1000 K) that is close to the characteristic temperature of the solid breeder in a fusion reactor [10,11], and 1500 K, a temperature well above the superionic phase transition (1200-1350 K [6,7,12]). Irradiation is modelled by creating primary knock-on Li atoms (PKAs) and we study the healing of the structure after irradiation and the saturation of the damage as a function of the number of PKAs.

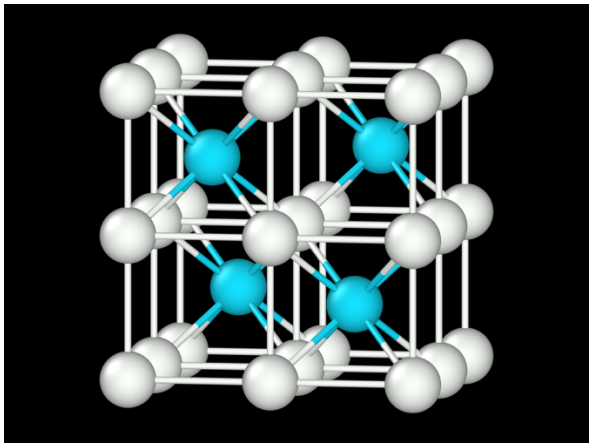

Figure 1. Unit cell of Li_2O. Blue spheres are oxygen atoms, white spheres are lithium atoms.

In Section II, Steinhardt order parameters are introduced and calculated for atoms located at "perfect" lattice sites and at interstitial positions in Li_2O. Section III introduces the concept of a distance metric for a given atom in the radiation-damaged material based on calculated Steinhardt parameters. In Section IV results of the molecular dynamics simulations are reported and discussed, before we conclude in Section V.

II. Steinhardt order parameters

Initially, Steinhardt order parameters (SOPs) were developed as a means of determining local bond-orientational order in liquids and glasses [9]. They have been used frequently to distinguish between different crystalline structures and local environments [13] and have been used previously as a measure of radiation damage [14,15]. It is important that these parameters are independent of the reference frame used to specify the crystal structure, i.e. they are translationally and rotationally invariant. Thus, they are a better method of quantifying the extent of damage in crystalline solids than simply monitoring the magnitudes of the displacements of the atoms, since these do not account for healing processes in which the original crystal reforms in some regions after the displacements.

Here, we measure the extent of the damage in lithium oxide by using the SOPs to

determine changes in local environments after repeated exposure to high energy PKAs, identifying defects such as vacancies and interstitials. Mickel *et al.* [16] have discussed several possible definitions of a "neighbourhood" of an atom. These define either a cutoff distance or fixed number of nearest neighbours; and here we have chosen the former. We consider two possible positions for the Li atom: (i) a lattice site in a simple cubic lattice and (ii) an interstitial position in a centre of an eight-atom Li cube. The number of neighbours and their corresponding distances from that atom are summarized in the Table 1.

Neighbour	Li in perfect lattice			Li in interstitial position		
	Distance	Type	Number	Distance	Type	Number
NN	$d\sqrt{3}/2$	O	4	$d\sqrt{3}/2$	Li	8
2NN	d	Li	6	d	O	6
3NN	$d\sqrt{2}$	Li	12	$d\sqrt{11}/2$	Li	24

Table 1. First three nearest neighbours (NN) of a Li atom in the perfect crystal, and of a Li atom in the interstitial position in a centre of an eight-atom Li cube.

From Table 1, the most natural cutoff distance is 1.2d (≈ 2.8 Å), thus covering the first and second but not the third nearest neighbours, for both positions of a Li atom. This defines the *primary sphere* of the atom. Li and O atoms both make up this *primary sphere*. When calculating the SOPs of Li atoms, the chemical identities of the atoms in the primary sphere are ignored.

SOPs are first calculated for each individual Li atom, selected in turn from the structure. The vectors $\mathbf{r_j}(r,\theta,\phi)$ which connect this atom i to its neighbour j, $1 \le j \le N_p$ where N_p is the number of neighbours in the *primary sphere* are calculated. For each vector a set of even-order spherical harmonics Q_{lm} are generated [17] and averaged over the N_p neighbours:

$$Q_{lm}(\boldsymbol{r_j}) = Y_{lm}(\theta(\boldsymbol{r_j}), \phi(\boldsymbol{r_j})) \qquad (1)$$

$$Q(i) = \frac{1}{N_p}\sum_{j=1}^{N_p} Q_{lm}(j) \qquad (2)$$

For each l, the $q_{lm}(i)$ are averaged over all the possible values of m to obtain a rotationally invariant quantity:

$$q_l(i) = \sqrt{\frac{4\pi}{2l+1}\sum_{m=-1}^{l}|Q_{lm}(i)|^2} \qquad (3)$$

The disorder in Li_2O predominately involves Li disorder, and so here we select only Li atoms as central atoms in the primary spheres. Table 2 shows the substantial differences between the SOPs for even l from 4 to 12 for a primary region of a sphere with radius 1.2d centred on a Li at a perfect lattice position (column 2) and those for a sphere of the same radius centred on an Li in interstitial position (column 3). SOPs for a primary region centred on a Li at a perfect lattice position but adjacent to an occupied interstitial (column 4), or for a primary region centred on a Li at a perfect lattice position but adjacent to a vacancy (column 5), also differ from the values shown in column 2, with especially large variation for q_{10}.

SOP	Li in perfect lattice position	Li in interstitial position	Li adjacent to occupied interstitial	Li adjacent to a vacancy
q_4	0.254588	0.0363696	0.201008	0.210602
q_6	0.463548	0.510688	0.483742	0.48699
q_8	0.515947	0.429322	0.496397	0.499511
q_{10}	0.0132062	0.195191	0.0991352	0.117909
q_{12}	0.4691	0.404799	0.453119	0.456713

Table 2: Comparison of calculated SOP values for a primary region defined by a sphere radius 1.2d centred on a Li atom at a perfect lattice position, those for a sphere of the same size centred on a Li occupying an interstitial position, centred on a Li adjacent to an occupied interstitial and adjacent to a vacancy.

We can therefore use the SOPs as a measure of the local environment of ions and hence of the number of interstitials in the damaged material. To test first the ability of SOPs to provide a physically realistic picture of disorder, and to see if it is sensitive enough to detect structural changes, we have used them to examine the disorder not in the damaged material but below and above the superionic phase transition temperature in

the absence of a PKA event. An NPT high-temperature molecular dynamics simulation was run using LAMMPS (Large-scale Atomic/Molecular Massively Parallel Simulator) program [18,19] and a small cubic simulation box of 768 atoms, followed by quenching the system to low temperature and calculating the SOPs of the Li atoms. The set of Buckingham potentials was taken from previous studies [8,20]. The simulation was performed at a temperature of 1500 K, well above the superionic phase transition. The Nose-Hoover thermostat was used, with a chain length of 3, damping parameter of 0.1 ps and a barostat with a damping parameter of 0.1 ps. The simulation was run for 10 ps using the velocity Verlet algorithm, followed by a static minimisation that was carried out to reduce the effects of atomic vibrations and the subsequent noise. SOPs were calculated from atomic positions at the end of the minimisation.

For the small simulation box used in this particular case, the disorder can be observed by eye, before being studied using the SOPs. The final snapshot of the simulation at 1500 K is shown in Figure 2. Arrows show one Li interstitial (Li atom in a row of O atoms), and one Li vacancy (seven Li atoms in a row of Li atoms where there should be eight). Overall, six Li interstitials and six vacancies were identified when viewed from different angles (but are obscured in this image).

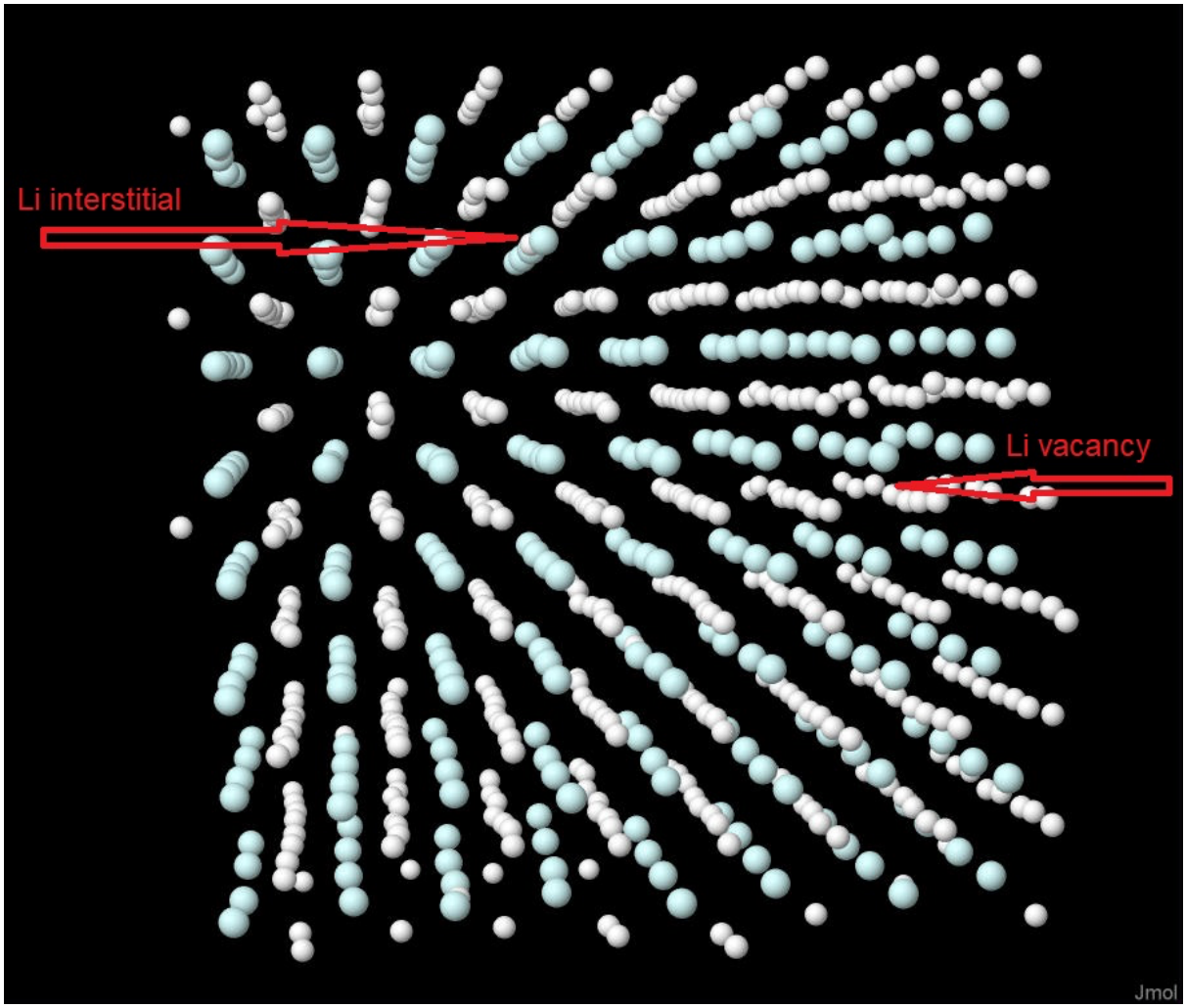

Figure 2. Final snapshot of the molecular dynamics simulation described in section II.

We now calculate SOP values and compare the information they provide to the qualitative visualisation. Our procedure here differs from that in previous work on pyrochlores, in which SOPs for regions within the cell were plotted as a histogram in order to classify the local structure as pyrochlore, defect fluorite and anion-disordered pyrochlore [14]. Here local environments are not classified in such a way and a different approach is required. We write the set of SOP values for a single Li atom as a 'coordinate' in a five-dimensional space $(q_4, q_6, q_8, q_{10}, q_{12})$, which we compare with the 'coordinate' SOP values of known environments. Two "distances" were calculated – between the SOP 'coordinates' of a Li atom in the simulation, and either the 'coordinates' of Li in a perfect lattice site $d_n(P)$, or in an interstitial position $d_n(I)$, as specified in Table 2:

$$d_n(P) = \left(\sum_{i=4}^{12}\left(q_i(n) - q_i(P)\right)^2\right)^{1/2} \qquad (4)$$

$$d_n(I) = \left(\sum_{i=4}^{12}\left(q_i(n) - q_i(I)\right)^2\right)^{1/2} \qquad (5)$$

where $q_i(P)$ and $q_i(I)$ stand for SOPs of Li in perfect and interstitial position, respectively, and the sum is restricted to even i. The points $(d_n(P), d_n(I))$ for all Li atoms can then be plotted on a two-dimensional graph, as in Figure 3.

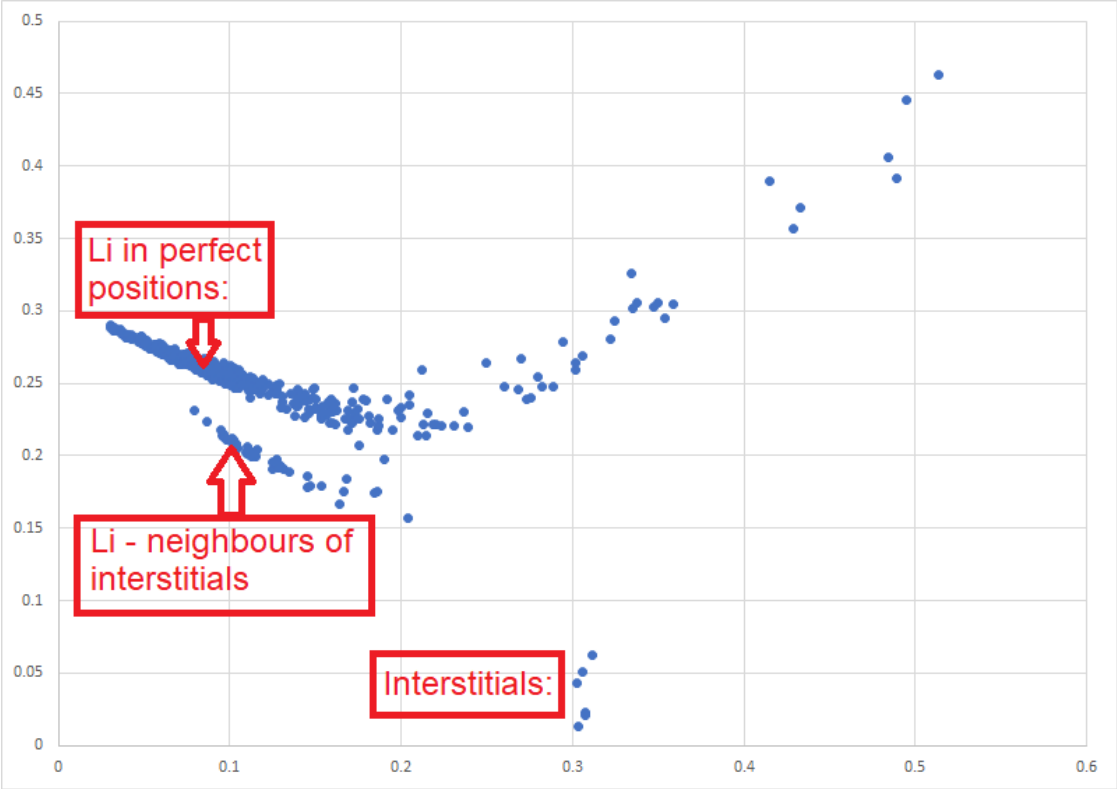

Figure 3. $d_n(I)$ vs $d_n(P)$, as defined in equations 4 and 5.

Atoms in perfect lattice positions should have an x-coordinate $(d_n(P))$ close to 0, while for interstitials, the y-coordinate $(d_n(I))$ should approach 0. Figure 3 shows that most Li atoms occupy perfect lattice positions, as also shown *qualitatively* in Figure 2. Indeed, in Figure 3 the six points with $d_n(P) > 0.3$ and $d_n(I) < 0.07$, were found to correspond to the six Li ions qualitatively observed to not occupy perfect lattice positions. This group is well separated from the lithium atoms in other environments. The data points in the remainder of the Figure 3 separate out atoms which are neighbours of atoms in interstitial positions. There is also a "tail" of points for which both $d_n(P)$ and $d_n(I)$ are large. These atoms correspond not to point defects, but to more distorted environments associated with the superionic phase. Thus, comparing the visual determination of the disorder in Li_2O in Figure 2 with the graphical representation in Figure 3, the SOPs give broadly the same interpretation.

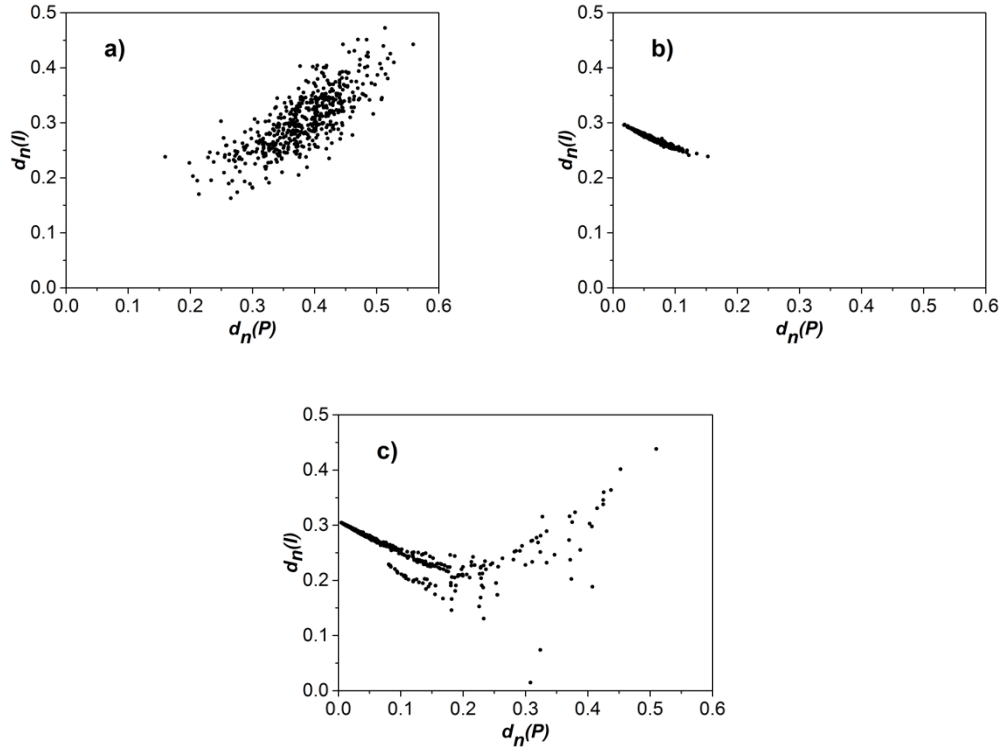

Figure 4. $d_n(I)$ vs $d_n(P)$, as defined in equations 4 and 5. Panels represent a) results for the final structure before any quenching or minimisation process b) results for the final structure obtained after subsequent quenching c) results for the final structure after subsequent minimisation.

We have investigated methods to reduce the noise caused by atomic vibrations evident for example in Figure 4a, in which $d_n(I)$ is plotted vs. $d_n(P)$ after 10 ps simulation and before any minimisation. One involves simply quenching at the end of the molecular dynamics run. In one test run, the system was gradually quenched to 100 K over 6 ps and then run at 100 K for a further 4 ps. This brings Li_2O below the superionic phase threshold temperature. The SOP analysis for the new final structure is shown in Figure 4b. The mean $d_n(P)$, $d_n(I)$ coordinate is (0.06, 0.27) and we conclude that almost all of the Li initially at non-lattice sites are back in perfect lattice positions. Such quenching thus has eliminated important defects and resulted in the system being close to a global energy minimum.

Static minimisation finding the nearest local (static energy) minimum is a better approach. The minimization was performed using the conjugate gradient algorithm until either relative change of energy between two steps was less than 10^{-8}, or until the final force on any component of any atom did not exceed 10^{-4} eV Å^{-1}. Results from this

approach are plotted in Figure 4c, which shows that a variety of local environments is maintained and allows us to identify Li in perfect lattice positions, interstitials and neighbours of interstitials. This also allows a clearer definition of a "cutoff" such that any particle with SOP values outside this cut off is considered displaced from its perfect lattice position. In particular, all Li atoms that are neighbours of interstitials have $d_n(P) > 0.05$. Accordingly, in the simulations of damage reported in the next section Li atoms are considered displaced if the distance $d_n(P)$ after minimisation was greater than 0.05. Of course, this choice is somewhat arbitrary; in particular Figures 4b and 4c demonstrate that there are atoms in perfect lattice positions that have $d_n(P) > 0.05$. Nevertheless, further simulations have shown that increasing the threshold value from 0.05 to 0.1 reduces the number of displaced atoms by approximately the same amount (30% to 40%) independently of the level of damage level, so that the *relative* number of displaced atoms in separate simulations remains the same and does not influence the conclusions.

IV. Simulations with high-energy Li atoms

A high energy neutron travelling through lithium oxide creates primary knock-on atoms with various energies. In an elastic collision, kinetic energy T that is transferred from neutron to the struck atom (recoil energy) is given by [21]

$$T = \frac{4mM}{(M+m)^2} E_i(1 - \cos\varphi)$$

where E_i is the kinetic energy of the incoming neutron, m and M the mass of the neutron and the atom respectively, and φ the scattering angle in the centre-of-mass system. The transferred energy thus decreases with increasing mass of the atom. In the case of Li_2O, the energy of lithium PKAs (atomic mass 6 or 7) will be 2.21 or 1.98 times that of oxygen PKA (atomic mass 16) for the same value of φ. For this reason, we considered only Li PKAs.

The extent of damage in Li_2O following a PKA event can be measured using SOPs as described earlier to determine the number of defects and comparing with the undamaged material. These simulations were run in the NPT ensemble with the

LAMMPS default Nose-Hoover thermostat and barostat in a large supercell of 16×16×16 cubic unit cells (32768 Li atoms and 16384 O atoms). After an initial run of 3 ps, one randomly chosen Li atom was given a high energy of 1 keV, simulating the PKA. A variable timestep was used to make sure that during the early steps of each cascade, the timestep was sufficiently short to allow for fast moving atoms with high kinetic energy, while ensuring overall resource efficiency at later stages of the MD run. The variable timestep did not allow the fastest atom in the simulation to move more than 5% of an interatomic distance during one timestep. Since the smallest interatomic distance in perfect Li_2O is close to 2.0 Å (Li-O), the constraint imposed was that the fastest atom does not move more than 0.1 Å in one timestep. For an initial PKA energy of 1000 eV, this corresponds to an initial timestep of 6×10^{-5} ps. As the PKA slowed down, the timestep gradually increased until it reached a limiting value of 1 fs. In the MD run less than 1 ps was always sufficient for the temperature to return to its initial value after the spike caused by the PKA. After 1 ps, another Li atom was randomly chosen and given an energy of 1 keV and so on. The simulations were performed with between 1 and 400 PKAs. After the runs with all the PKAs were completed, runs with lengths varying between 1 and 1024 ps were performed as discussed below and the energy then minimized. A plot of $d_n(P) - d_n(I)$ was then used to estimate the degree of disorder in the system. Runs were carried out at three temperatures: 500 K (low), 1000 K (close to the working temperature of the breeder blanket), and 1500 K (high, above the superionic transition).

Initially, simulations of length 1 ps were run after creating each PKA in order to find whether the level of damage keeps increasing or saturates as a function of the number of PKAs. Li and O atoms were considered displaced if the distance $d_n(P)$ was greater than 0.05, as discussed earlier. The number of displaced atoms after minimization as a function of the number of PKAs at 1000 K is shown in Figure 5. Results for both Li and O show a clear trend towards saturation after about 100 PKAs. This trend agrees with several recent computational studies showing damage saturation in metals, namely Fe, W [22] and Mo [23], as well as an experimental study of W [24]. These have indicated saturation at a level of damage around 0.1 – 0.2 dpa (displacements per atom). While displacement per atom is a rather crude measure of damage, it is possible to estimate it from our simulations using the Kinchin-Pease formula as modified by

Norgett, Robinson, and Torrens [25] for the number of created vacancies v [26]:

$$v(T) = \frac{0.8\,T}{2E_d} \tag{6}$$

T is the kinetic energy of the PKA and E_d the displacement threshold energy. As an estimate of E_d in Li_2O, the threshold displacement energies of Li and O in $LiAlO_2$ (22 eV for Li, 37 eV for O, as estimated in [27]), were used. With T = 1000 eV, this corresponds to the creation of between 11 and 18 vacancies per PKA. In this case, 100-400 PKAs would result in the creation of 1100-7200 vacancies, i.e., a dpa of about 0.05-0.2, in line with the results for metals.

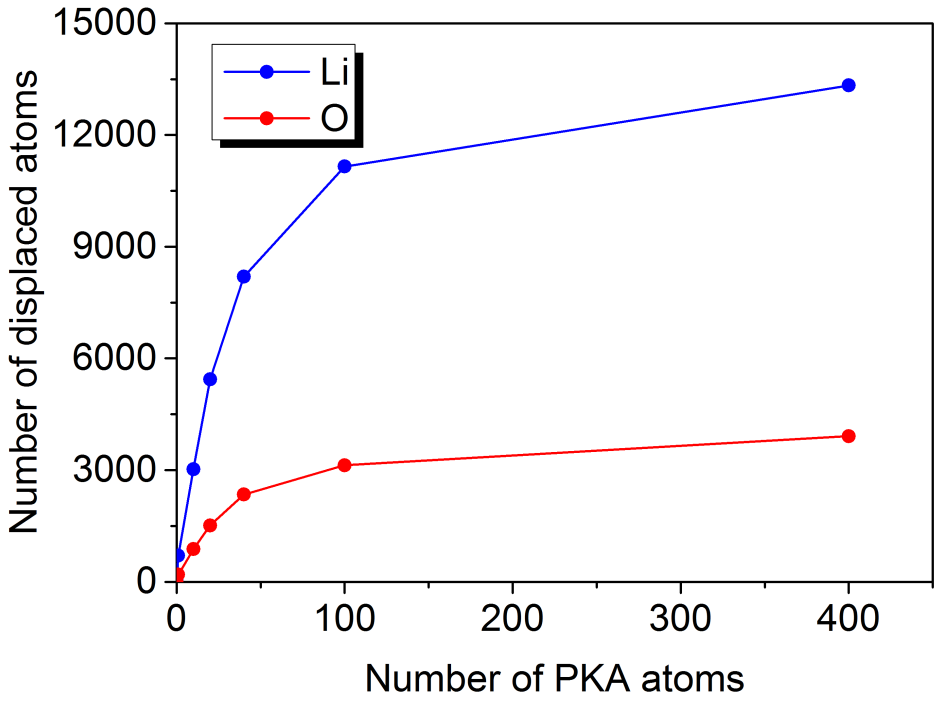

Figure 5. Number of displaced Li and O atoms after the 1 ps simulation runs and subsequent energy minimization, as described in the text, vs. the number of PKAs at 1000 K.

We note that simulations at 500 K give a very similar picture, while at high temperature, 1500 K, the number of displaced atoms almost does not depend on the number of PKAs. Simulations at 1500 K without PKAs give about 12000 displaced Li atoms after minimisation, confirming that at this temperature, Li_2O is superionic. The difference in damage creation at different temperatures are clear in Figure 6, where plots of $d_n(I)$ vs $d_n(P)$ after a single PKA atom creation and one 1 ps run are shown.

Next, the decrease of damage with time was studied. After between 1 and 100 PKAs

were fired with a time of 1 ps between each firing, the system was left to relax between 1 and 1024 ps before minimisation. In Figure 7 the number of displaced Li atoms as function of relaxation time at 1000 K is shown. There is a clear reduction of damage in each case. However, with increasing number of PKAs, the rate of decrease in damage slows down and the time needed to return to the level of disorder that exists in the undamaged system (i.e., no PKA firing) increases. These time dependencies can be rather accurately fitted using power laws. Denoting the time-dependent number of displaced Li atoms as $D_{Li}(t)$, the power law can be written as

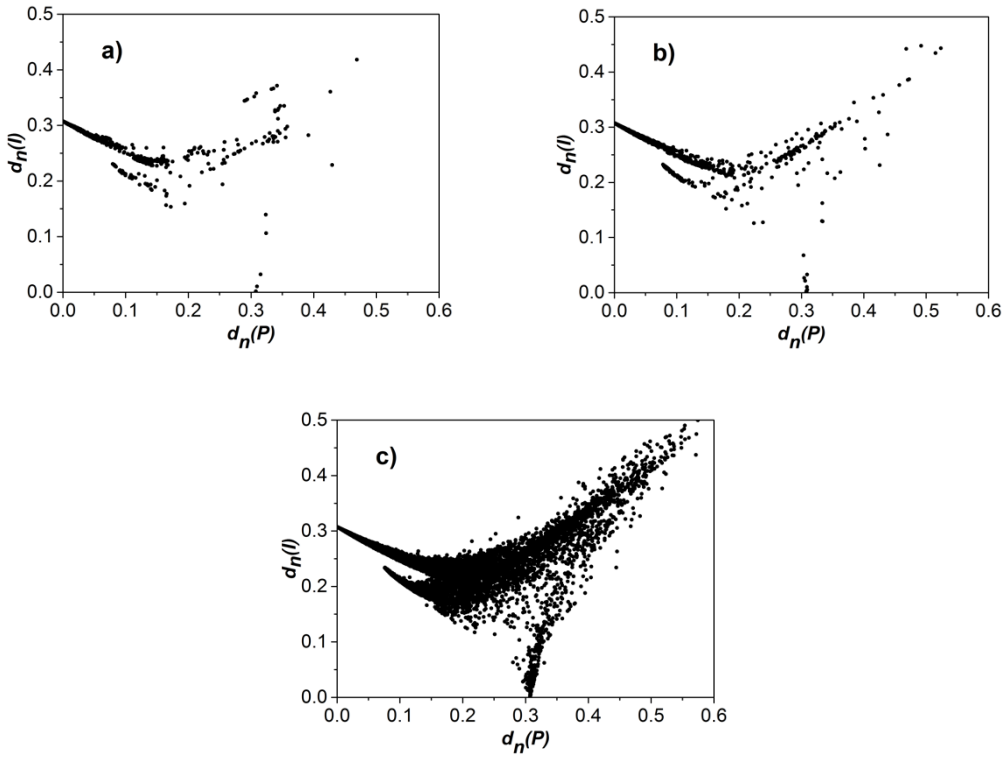

Figure 6. $d_n(I)$ vs $d_n(P)$ at different temperatures after creation of a single PKA atom and a 1 ps run followed by minimisation. Temperatures are (a) 500 K, (b) 1000 K and (c) 1500 K.

$$D_{Li}(t) = D_{Li}(0)t^{-\alpha} \qquad (7)$$

In Table 3, we show parameters of the fit ($D_{Li}(0)$ and α), as well as R^2, the measure of goodness of the fit. The power-law exponent α decreases with increasing number of PKAs, resulting in the slowing down of damage recovery. With no PKAs, our simulation produces 59 displaced atoms in the simulation box at 1000 K. Using the results from Table 3, after a single PKA about 200 ns are needed to return to this amount. This time for recovery increases substantially for higher number of PKAs. For 10 PKAs, we estimate about 0.003 s, and for 20, 40, and 100 PKAs even longer times.

Realistically this means that under the conditions of neutron irradiation, the state that corresponds to no PKAs is never reached, and the system at some point in time reaches a steady state of constant (permanent) irradiation-related disorder.

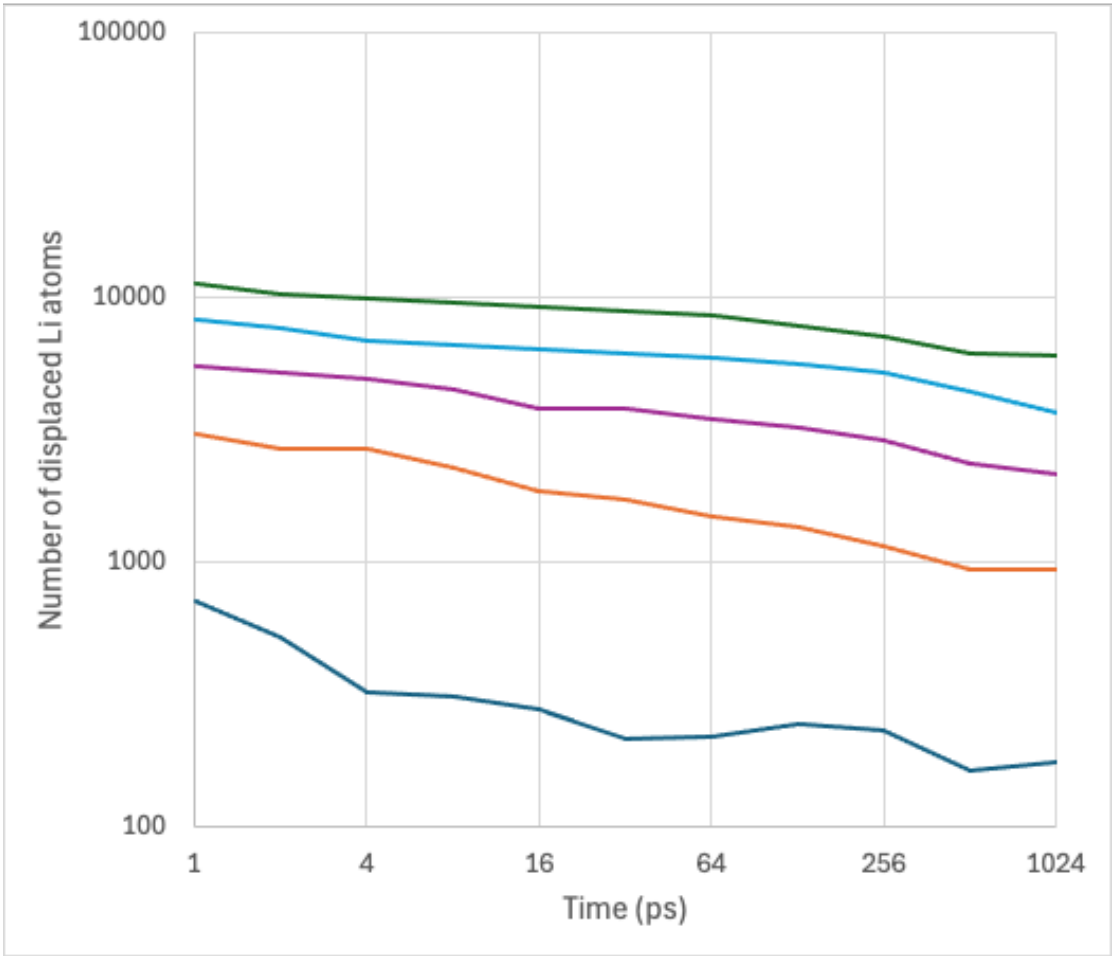

Figure 7. The number of displaced Li atoms $D_{Li}(t)$ as a function of time for 1 (dark blue), 10 (orange), 20 (dark red), 40 (light blue), and 100 (green) PKAs at 1000 K.

Number of PKAs	$D_{Li}(0)$	α	R^2
1	508.74	0.176	0.8134
10	3149.7	0.182	0.983
20	5743.5	0.134	0.9774
40	8251.7	0.098	0.9428
100	11275	0.086	0.9618

Table 3. Power-law fit parameters and the value of R^2 for time-dependent damage reduction with different numbers of PKAs, at 1000 K.

The same simulations were performed also at temperatures 500 K and 1500 K. At 500 K, a similar power-law dependence was found, but with different values of fit parameters, as shown in Table 4. The number of displaced Li atoms immediately after creation of all PKAs $D_{Li}(0)$ is, as expected, close to that at 1000 K, but the power-law exponent α is substantially lower than at higher temperature, resulting in much longer recovery times. Under permanent neutron irradiation, therefore, the resulting steady state disorder will be higher at 500 K than at 1000 K.

Number of PKAs	$D_{Li}(0)$	α	R^2
1	363.62	0.038	0.811
10	2922.2	0.092	0.9731
40	8059.7	0.053	0.9798
100	12672	0.031	0.9859

Table 4. Power-law fit parameters and R^2 value for time-dependent damage reduction at different number of PKAs, at 500 K.

At 1500 K, above the superionic transition, we do not see any change of the damage level with time. In the undamaged material, $d_n(P) > 0.05$ for about 12500 atoms at this temperature. For comparison, at 1000 K only 59 atoms have $d_n(P) > 0.05$ at the end of the simulation. The number of distorted atoms at 1500 K increases further compared to that in the undamaged material to about 18700 atoms after the creation of 40 PKAs, and subsequently no decrease of their number was effectively observed during the length of the simulation, as can be seen in Figure 8.

Overall, comparison of the damage evolution at the three temperatures suggests that the healing at 500 K is slowed down because of the low temperature, and that at 1500 K no healing is observed during the characteristic timescale of the molecular dynamics simulations. Healing is fastest at 1000 K. This suggests the existence of a temperature close to 1000 K, at which the healing of the damaged crystal is fastest.

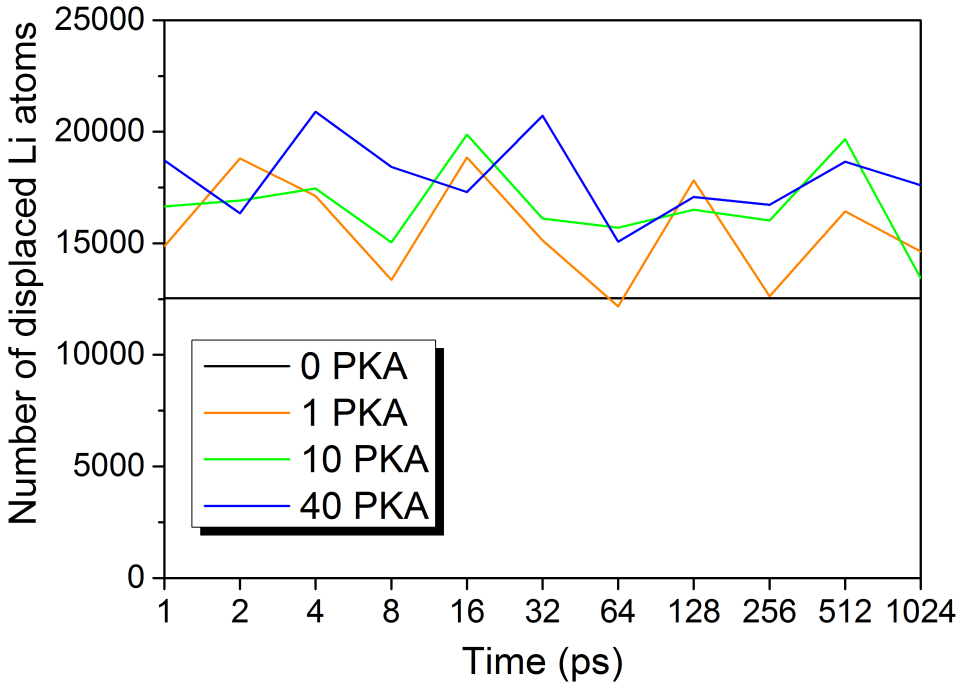

Figure 8. The number of displaced Li atoms $D_{Li}(t)$ as a function of time for 1, 10, and 40 PKAs at 1500 K, above the transition to superionic phase. Number of displaced atoms in undamaged Li_2O (0 PKA) is shown as the dark blue line.

V. Conclusions

We have extended further the use of Steinhardt order parameters, initially devised for analysing differences in structure between monoatomic systems, for the analysis of damage and disorder in polyatomic crystals, in this case in lithium oxide. We have developed a classification scheme in which atoms can be classified as displaced based on the values of a "distance" between their positions and the perfect values in Steinhardt-order-parameter space. With increasing number of PKAs, the damage in the system increases but begins to saturate when the number of PKAs leads to damage of the order of 0.05 – 0.2 dpa. This is in agreement with what has been found experimentally for metals. After irradiation, the system begins to recover, and the number of displaced atoms decreases. The rate of the decrease, i.e., the healing, is highest at 1000 K. In contrast, at temperatures above the superionic phase transition, the rate of healing falls to the extent that no recovery was seen during the molecular dynamics simulations. At 500 K, on the other hand, the rate of healing is lower because of the slower diffusion. Under the conditions of constant neutron irradiation, the

resulting steady state disorder thus will be lowest at 1000 K. It is important to keep structural disorder as low as possible, because increasing damage results in breeding material swelling, cracking, and may lead to a decrease in the breeding rate and/or a need to replace the material. Further experimental and simulation studies should pin down the working temperature of the Li_2O breeder around 1000 K that results in the slowest accumulation of damage. Steinhardt order parameters will be useful more widely in the study of defects, damage and healing in other materials under irradiation.

Acknowledgements

This work was carried out using the computational facilities of the Cambridge Service for Data Driven Discovery (CSD3) - https://www.csd3.cam.ac.uk. To obtain further information on the data and models underlying this paper please contact PublicationsManager@ukaea.uk.

References

1. J. G. van der Laan *et al., J. Nucl. Mater*. **283-287**, 99 (2000).

2. M. J. Sadowski, Nukleonika **60**, 331 (2015).

3. F.A. Hernández and P. Pereslavtsev, *Fus. Eng. Des.* **137**, 243 (2018).

4. B. M. Tripathi, A. K. Tyagi, and D. Prakash. Synthesis and Processing of Li-Based Ceramic Tritium Breeder Materials. In: Tyagi, A.K., Ningthoujam, R.S. (eds) Handbook on Synthesis Strategies for Advanced Materials. Indian Institute of Metals Series. Springer, Singapore, 2021. https://doi.org/10.1007/978-981-16-1892-5_18

5. D. Taylor, *British Ceramic Transactions and Journal* **83**, 32 (1984).

6. S. Hull *et al., J. Nucl. Mater*. **160**, 125 (1988).

7. T.W. D. Farley *et al., J. Phys.: Condens. Matter* **3**, 4761 (1991).

8. M. Yu. Lavrentiev, N. L. Allan, and C. Wragg, *Phys. Chem. Chem. Phys.* **21**, 14964 (2019).

9. P. J. Steinhardt *et al*., *Phys. Rev. B* **28**, 784 (1983).

10. G. Piazza *et al., Fus. Eng. Des.* **58-59**, 653 (2001).

11. A. R. Raffray *et al., J. Nucl. Mater*. **307-311**, 21 (2002).

12. Y. Oishi *et al., J. Nucl. Mater*. **87**, 341 (1979).

13. D. Moroni *et al.*, *Phys. Rev. Lett.* **94**, 235703 (2005).

14. A. Archer *et al.*, *J. Phys Condens. Mat.* **26**, 485011 (2014).

15. A. Archer *et al.*, *Mol. Simul.* **47**, 273 (2021).

16. W. Mickel *et al., J. Chem. Phys.* **138**, 044501 (2013).

17. P. M. Morse and H. Feshback, *Methods of Theoretical Physics*. (McHraw-Hill Book Company, Inc., New York, Toronto, London, 1953).

18. A. P. Thompson et al., *Comp. Phys. Comm.* **271**, 10817 (2022).

19. www.lammps.org

20. R. M. Fracchia *et al., J. Phys. Chem. Solids* **59**, 435 (1998).

21. G. S. Was, *Fundamentals of Radiation Materials Science* (Springer, Berlin, Heidelberg, New York, 2007).

22. P. M. Derlet and S. L. Dudarev, *Phys. Rev. Materials* **4**, 023605 (2020).

23. M. Yu. Lavrentiev *et al., J. Appl. Phys.* **132**, 125902 (2022).

24. A. Hollingsworth *et al., J. Nucl. Materials* **558**, 153373 (2022).

25. M. J. Norgett, M. T. Robinson, and I. M. Torrens, *Nucl. Eng. Des.* **33**, 50 (1975).

26. G. H. Kinchin and R. S. Pease, *Rep. Progr. Phys*. **18**, 1 (1955).

27. H. Tsuchihira, T. Oda, and S. Tanaka, *Nucl. Instruments Methods Phys. Res. B* **269**,

1707 (2011).